J. Appl. Comput. Mech., xx(x) (2024) 1-14
DOI: 10.22055/jacm.2024.46183.4473

ISSN: 2383-4536
jacm.scu.ac.ir

Shahid Chamran University of Ahvaz

Journal of Applied and Computational Mechanics

Research Paper

Influence of Curvature Radius on Mechanical Behavior of Extruded 6061-T6 Aluminum in Roll Bending

Mauricio da Silva Moreira[1], Carlos Eduardo Marcos Guilherme[1], João Henrique Corrêa de Souza[1], Elizaldo Domingues dos Santos[1], Ana Pavlovic[2], Liércio André Isoldi[1]

[1] Federal University of Rio Grande - FURG, Rio Grande, Brazil, Itália Avenue km 8, Rio Grande, 96203-900, Brazil,
Email: mauriciodsm6@gmail.com (M.S.M.); carlosguilherme@furg.br (C.E.M.G.); joaoh_cs@hotmail.com (J.H.C.S.); elizaldosantos@furg.br (E.D.S.); liercioisoldi@furg.br (L.A.I.)

[2] Department of Industrial Engineering, University of Bologna, Viale del Risorgimento, Bologna, 40136, Italy, Email: ana.pavlovic@unibo.it

Received February 19 2024; Revised May 09 2024; Accepted for publication June 07 2024.
Corresponding author: A. Pavlovic (ana.pavlovic@unibo.it)

Abstract. This article presents a numerical study encompassing the mechanical behavior prediction during the roll bending process applied to four distinct profiles of extruded 6061-T6 aluminum, considering different radii of curvature. The numerical simulations were conducted using the ANSYS® software, based on the finite element method, adopting the three-dimensional SOLID187 finite element. The employed computational model was developed and validated by Moreira et al. [1]. The obtained results demonstrate consistent patterns regarding stresses and displacements for the different radii of curvature. As the radius of curvature decreases, the von Mises stress tends to increase, approaching the material's strength limit. This phenomenon is critical for identifying points of maximum stress and ensuring adequate safety margins to prevent structural failures. Displacements along the profiles were also monitored, providing relevant information about its evolution at different radii of curvature and allowing curve fitting for these displacements in each profile investigated. Therefore, these consistent patterns observed can help to determine the direct influence of curvature on resulting defects, contributing to an in-depth understanding of the mechanical behavior of these profiles.

Keywords: Extrusion, Roll bending, 6061-T6 aluminum profiles, radius of curvature, Finite Element Method, SOLID187.

1. Introduction

Profiled aluminum profiles are an excellent choice for structural applications that require high strength and lightness, combined with the ability to shape the material into complex and precise forms. These profiles are widely used in various sectors, including aerospace, automotive, maritime, and construction. Due to its excellent mechanical properties, aluminum has been the preferred material in many structural applications, especially when corrosion resistance is a critical factor. Additionally, cold-formed aluminum profiles are lighter than equivalent steel sections, enabling the fabrication of lighter and more cost-effective structures. Among the different types of aluminum, the extruded 6061-T6 aluminum is a widely employed alloy in maritime, aerospace, civil, and automotive applications, owing to its properties such as corrosion resistance, high mechanical strength, lightweight, good weldability, and fatigue resistance [2, 3].

In the scientific literature, there is a notable absence of studies on the roll bending process of aluminum profiles. In contrast, the roll bending of steel profiles has been extensively studied and documented, reflecting a well-established research tradition in this area. Moreover, the majority of these works employs the Finite Element Method (FEM) as approach to numerically simulate the mechanical behavior, as in [4-13]. Besides that, an important aspect in this type of mechanical forming problem is related to the contact between the construction materials involved, as discussed in [14-17].

Among the studies related to the topic of this work, it is worth highlighting the research by Hansen and Jannerup [18], who focused on understanding the geometric aspects of the three-roll beam bending process, assuming a triangular distribution of the moment between the rollers. The primary objective of the research was to obtain a more accurate geometric model for controlling the bending process, formulating a method to determine the position of the upper roll in accordance with the desired curvature function. The research revealed significant results, demonstrating the possibility of calculating the beam's curvature during bending with notable agreement with the experimentally determined curvature function. Calculated functions differed substantially from commonly assumed constants, enriching the understanding of the roller bending process in beams. A practical and relevant aspect emerged by demonstrating that, contrary to common practice involving trial and error in manual control, calculations based on the formulated model allowed precise determination of the machine's geometry. This resulted in final curvature deviations of around 5% to 10% for the considered curvature range. Sensitivity analysis highlighted that the roller bending process is more sensitive to variations in machine geometry than material characteristics, especially within the considered curvature range. This observation is crucial for enhancing process parameter control and identification.

Published online: June 20 2024

Another relevant study was conducted by Gandhi and Raval [19], presenting a mathematical model aimed at predicting the load on the upper cylinder needed to pre-bend a plate in a three-roll bending machine. Analytical displacements of the upper cylinder were calculated based on specific bending load data for that cylinder, considering different compositions of steel plates. The pre-bending stage was analyzed using a numerical approach in LS-Dyna's Hyperform software. A two-dimensional finite element model, incorporating the symmetry condition of the plate rolling process, was adopted to optimize the solution time. In the simulation, C-Mn steel plates with SA-387Gr11C12 material grade were used. To deepen the understanding of the friction coefficient's impact on the pre-bending load, numerical simulations were conducted considering five distinct values of this coefficient at the plate-roller interfaces. The results revealed a positive correlation between the friction coefficient and the pre-bending load, indicating that an increase in this coefficient leads to a proportional increase in the load required for pre-bending the plate.

Tailor and Gandhi [20] conducted a finite element analysis of the three-roll bending process. The study investigated the influence of various parameters on the quality of bent sheet metal, including roll positions, rolling speed, sheet material, sheet length, and friction at the interfaces between the rolls and the sheet. The work involved detailed numerical simulations performed in a specific software environment, such as Hyperform LS-DYNA, aiming to gain a better understanding of the deformation process and enhance the efficiency and accuracy of sheet metal bending operations.

Merklein et al. [21] investigated the three-roll bending process of metallic tubes using the three-roll technique. In this study, a computational model developed for three-roll bending was described, and the initial results of numerical investigations conducted on steel tubes made of St37 carbon steel were presented. The finite element analysis focused on modeling tool stiffness, describing the kinematics of the adjusting roll, and characterizing material behavior for simulation. The results of numerical investigations were compared with experiments conducted using a computer numerically controlled (CNC) bending machine available at the Chair of Manufacturing Technology at the University of Erlangen. The tube radius on the extrados and the bending angle were chosen as the primary criteria for validating the finite element model. The part geometry was measured using optical and tactile measurement devices.

Spoorenberg et al. [22] conducted the static analysis of a steel I-beam using the constraint method through finite element analysis. The study included numerical examples with different radii of curvature of the rolled profile, aiming to obtain residual stresses from the process. Two types of finite elements in the ANSYS® software, SOLID45 and SOLID95, were used to model half of the geometry, with the imposition of a symmetry boundary condition. The authors validated the numerical model with experimental data.

Zhao et al. [23] analyzed the stress and springback behavior of API X70 steel tubes during the three-roll bending process. Employing the finite element method, the authors mapped the curvature radii and stress within the workpiece during forming, providing numerical guidelines for roll system configuration to enhance production efficiency and product quality. The results underscored the importance of appropriately choosing forming parameters to obtain products with desired radii, observing a gradual springback process, and noting that changes in the three-roll system configuration did not significantly alter the final residual stress. Additionally, a neutral axis displacement of up to 2.0% of the thickness towards the compression side during the forming process was observed.

Feng and Champliaud [24] developed a computational model to analyze the asymmetric three-roll forming process. The study aimed to investigate stress and strain distribution during the forming process in steel and evaluate the influence of asymmetry on the final product's quality. A numerical simulation model based on plasticity theory was used to analyze stress and strain distribution at different stages of the forming process. The model considered roller geometry, material mechanical properties, and the influence of asymmetry on stress and strain distribution. The obtained numerical results showed that the asymmetry in the forming process can lead to a non-uniform distribution of stresses and strains along the plate. Additionally, the simulation allowed the final geometry of the formed plate to be determined, including the height of the formed piece and the final radius of curvature. Finally, numerical and experimental results were compared, with a deviation of less than 6%, leading the authors to conclude that the developed numerical simulation model can be used to predict stress and strain distribution in an asymmetric three-roll forming process.

Thakare et al. [25] developed a mathematical model to predict the displacement of the upper cylinder in the bending process of steel materials. Geometric, operational, and material parameters were considered for modeling. The percentage variation between experimental results and predicted values was also determined. Based on the results obtained with the developed model, it was possible to state that the model is accurate and reliable, with a percentage variation of less than 5%.

In the study of Thanasoulas and Gantes [26], residual stresses in rolled steel members, specifically in circular hollow sections (CHS), were investigated. Detailed finite element models were developed, taking into account geometric, contact, and material nonlinearities. To assess how bending characteristics affect stress and strain distributions, a parametric study was conducted considering parameters such as CHS diameter and thickness, bending radius, steel yield strength, bending length, bending roll diameter, and encapsulation angle of the bending matrix. Variation in residual stress formations was observed, attributed to the presence of transverse and shear stresses in the CHS workpiece within the three-point bending length. Finally, the obtained residual stress distributions were summarized, and a characteristic distribution was proposed based on the most commonly encountered plastic deformations.

Zhigulev et al. [27] researched the molding process of the three-roll bending, based on elastoplastic bending, on a three-roll bending machine. The study investigated physical models of the deformation zone during the interaction of the workpiece with the rolls, considering two stages: when the upper roll is moved without rotating the rolls and when the three rolls are rotated without moving the upper roll. The results of an experimental study of the deformation zone parameters are obtained and used to determine the profile of the tubular billet during molding on a specialized bending machine for the two stages of the bending process. The experiments showed that, for the first bending stage, the billet in the upper roll separation zone has a complex curvature and symmetric three-point and four-point contacts with the rolls. The second bending stage, with roll rotation, is characterized by an asymmetric deformation zone during three-point contact. Finally, regression equations for the geometric parameters of the profile sections of the bent piece are obtained.

Kamas and Sarıkaya [28] addressed the dynamic deformation analysis of a workpiece in the three-roll bending process using finite element simulation. An explicit dynamic model with two different 3D geometries, including cylindrical and convex bottom and side rolls, was developed. The computational model was validated with experimental results, demonstrating similar deformation outcomes. Aiming to avoid trial-and-error experimental costs, various parameters were varied in the simulation, such as geometry, element size, mass scaling factor, and rotation speed. The study emphasizes the importance of the mass scaling factor in minimizing computational costs, allowing for an increase in the time step of the explicit dynamic simulation. However, it is highlighted that excessive reduction of the simulation time can lead to non-physical consequences. Despite attempts to alter the design and reduce speed, distortion could not be avoided.

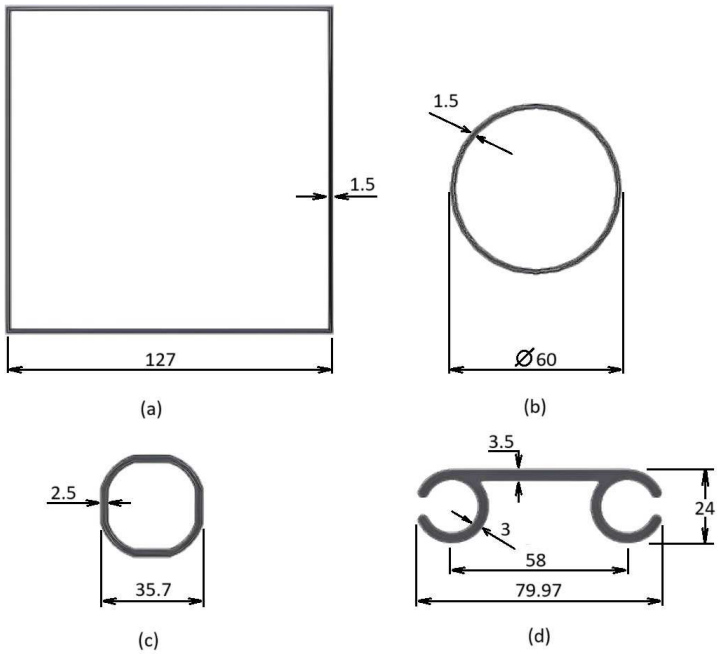

Fig. 1. Representation of the extruded 6061-T6 aluminum profiles (in mm): (a) profile 1; (b) profile 2; (c) profile 3; and (d) profile 4.

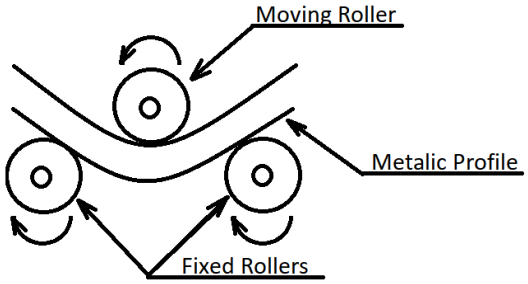

Fig. 2. Pyramid roll bending machine.

Finally, Mazur et al. [29] developed the analysis of the accuracy of measuring curved profiles with a coordinate measuring machine (CMM). The purpose was to determine the effect of scanning speed on the measurement results of shape deviation, assessment of measurement uncertainty of deviation, and measurement repeatability. During the profile scanning, three parameters were adjusted: scanning speed, permissible deflection of the probe, and scanning step. The results showed significant differences between the actual scanning speed and the defined values, as well as observations on measurement uncertainty and the influence of probe deflection on the results.

Based on that, the present work describes a numerical analysis of the roll bending process of four extruded 6061-T6 aluminum profiles, concerning the influence of different radii of curvature on its mechanical behavior. The study employs numerical simulation in the ANSYS® software, based on three-dimensional SOLID187 finite elements, with a computational model previously validated in Moreira et al. [1]. The main goal is to investigate the maximum von Mises stress and displacements in the cross-sections of the profiles when subjected to the roll bending process.

2. Materials and Methods

In this section, a brief explanation of the roll bending process for rolled profiles will be presented, along with the definition of the parameters necessary to develop the computational model and perform the numerical simulations.

Figure 1 depicts the cross section of the different aluminum profiles investigated in this study. The profile 1 (see Fig. 1(a)) stands out in structural applications. The square shape provides additional stiffness, making it an efficient choice in construction elements requiring strength and stability. In civil and architectural engineering projects, the square tube finds space in the composition of robust structures, offering a balance between efficiency and aesthetics. The profile 2 (see Fig. 1(b)) is used in various applications, such as the construction of lightweight structures like stair rails and handrails. This kind of profile is also applied in the automotive industry to reduce vehicle weight, promoting greater fuel efficiency; and in the manufacturing of sports equipment, such as bicycles and motorcycles, as well as in mounting systems, displays, and modular structures. In turn, the profile 3 (see Fig. 1(c)) plays a fundamental role in the transportation sector, specifically in semi-trailers used in tarpaulin processes. In this context, the profile is attached to the structure along with other components, forming an assembly that allows the tarpaulin to be securely fastened to the transported load. This application is widely used in semi-trailers to ensure safe transport and protection of the load during journeys. This profile is also applied in support structures for acrylic and polycarbonate sheets. Finally, the profile 4 (see Fig. 1(d)) is designed specifically as support for solar panels, standing out as a specialized solution in the implementation of photovoltaic systems. This profile is carefully designed to play an important role in the efficiency and stability of solar installations.

It is possible to highlight that the computational modeling of the roll bending process of aluminum profiles can be considered as an essential tool to ensure the quality and performance of these components. The numerical approach directly contributes to improving the safety and efficiency of each profile's distinct applications [30], justifying the carrying out of this work.

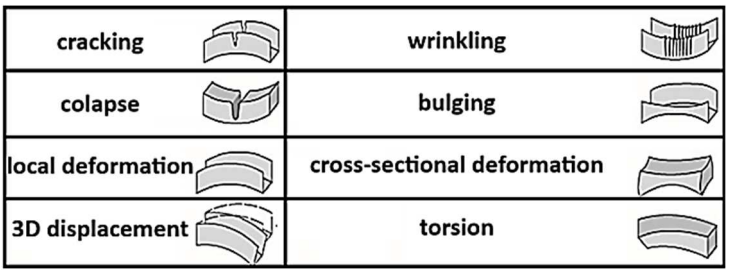

Fig. 3. Mechanical defects in curved profiles [33].

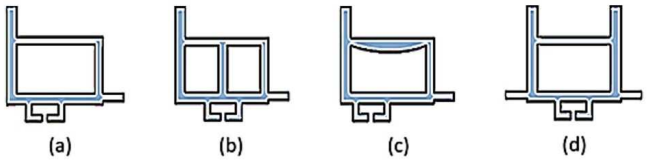

Fig. 4. Modifications to reduce deformation and twisting of the cross-section: (a) initial cross-section; (b) insert web; (c) increase wall thickness; and (d) reduce asymmetry [34].

2.1. Roll Bending Process

Figure 2 illustrates the common structure of a pyramid roll bending machine, which typically includes three rollers: one movable roller in the middle and two fixed outer rollers. The curvature of the profile is generated by the movement of the central roller between the two fixed rollers, and the passage of the profile through the three rollers causes a permanent deformation in the cross-sectional area [31].

According to Kissell and Ferry [2], the roll bending is a mechanical forming process used in metallic profiles (steel, copper, aluminum, among others) that allows profiles to be bent into complex shapes, such as arcs and variable curves.

2.2. Defects Originated in the Manufacturing of Curved Profiles

Curved profiles are predominantly produced through a subsequent bending process of semi-finished straight profiles, which are favorably obtained from billets through conventional extrusion. Similar to the bending of metal sheets, the phenomenon of elastic springback occurs during the bending process of profiles due to the presence of residual stress, resulting in geometric deviation and decreased bending accuracy. Residual stresses are characterized as those that persist in the material after the original cause of stress is removed, induced by various mechanisms, including inelastic (plastic) deformations in cold forming processes or non-uniform/high-temperature gradients/thermal incompatibility in hot forming/manufacturing processes [32].

Furthermore, during the profile bending process, specific defects manifest, such as deformation in the cross-section, twisting of asymmetric cross-sections or symmetric profiles along non-principal axes, and instability of profile walls (rippling). Additionally, large induced deformations, especially on the extrados, have the potential to degrade the metallurgical structure [33]. These mechanical defects are illustrated in Fig. 3.

The transverse deformation of profiles emerges as the main challenge in profile bending, becoming more critical with the increase in cross-sectional complexity and tighter geometric specifications. The twisting of the cross-section occurs during the bending of asymmetric profiles, where the center of gravity (CG) and the center of shear (CS) of the cross-section do not coincide [33]. Modifications in accordance with a suitable production design can be implemented in the cross-section to reduce its deformation and twisting [34], as illustrated in Fig. 4. The fundamental aspect of these modifications is the enhancement of profile stiffness and the reduction of asymmetry (decreasing the distance between CG and CS), which can be achieved by including webs as well as increasing wall thickness. Both actions enlarge the cross-sectional area and add weight to the structure.

Regarding the admissible displacements in cross-sections of aluminum profiles, they can vary considerably based on the application, the nature of the structure, and the loads involved. The Eurocode 9 [35] provides general guidelines on the design of aluminum structures but does not specify absolute values of allowable deformations or displacements, since these criteria tend to depend on the purpose and context of the structure in question. The limits of allowable displacements may vary according to several factors, including: (i) Type of structure: displacement requirements can vary significantly between structures such as buildings, bridges, industrial equipment, among others; (ii) Structural function: the function of the structure and the levels of load it must support will affect the allowable displacement limits. Critical safety structures, for example, may have stricter displacement criteria; (iii) Service conditions: if the structure is subject to permanent or variable loadings, allowable displacements may be defined differently; and (iv) Comfort and aesthetics: some structures may have specific criteria related to human comfort and aesthetic appearance, influencing the limits of allowable displacement. Therefore, to determine specific values of allowable displacements for aluminum profiles, it is necessary to take into account the guidelines of Eurocode 9 [35] and also the national standards or specific regulations of the country where the structure will be used.

2.3. Computational Modeling

The Finite Element Method (FEM) is widely used to perform structural analyses. Various computer programs employ this numerical method to solve different engineering problems, such as the ANSYS® Mechanical software, which was used in this work. This program offers several options for structural analysis, including static (linear and nonlinear), modal, spectral, dynamic, and buckling analysis. In all these analyses, nodal displacements are the main calculated variables, while other quantities such as strains, stresses, and reaction forces are derived from these displacement values obtained earlier for the entire computational domain [36].

Based on Spoorenberg et al. [22], a computational model considering the symmetry of the profile's cross-section was developed and validated in Moreira et al. [1] and will be used here. Therefore, due to the symmetry boundary condition adopted the geometry and dimensions of half of each profile presented in Fig. 1, as well as the rollers, are shown respectively in Figs. 5 to 8.

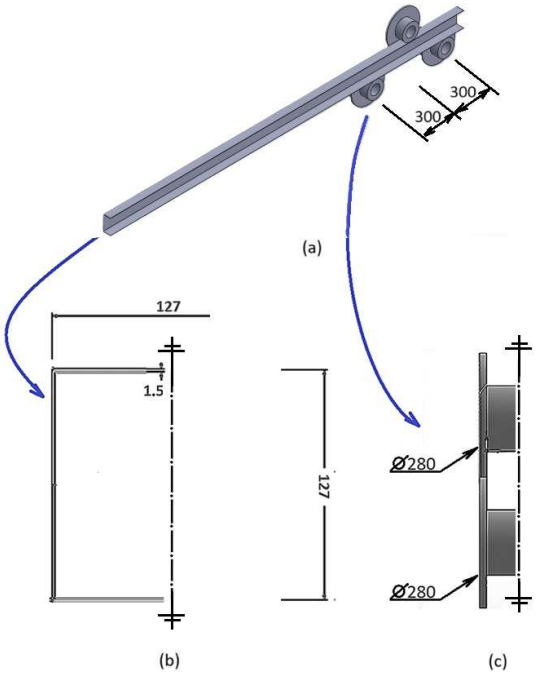

Fig. 5. Profile 1: (a) computational domain; (b) profile dimensions considering symmetry; and (c) rolling mill dimensions (in mm).

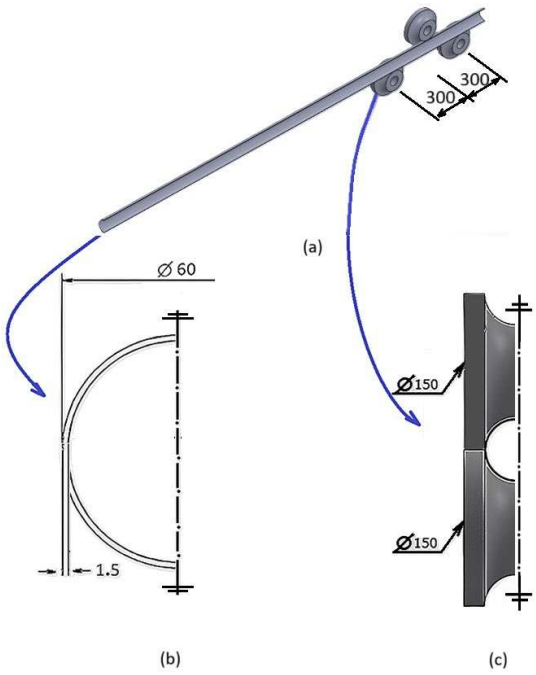

Fig. 6. Profile 2: (a) computational domain; (b) profile dimensions considering symmetry; and (c) rolling mill dimensions (in mm).

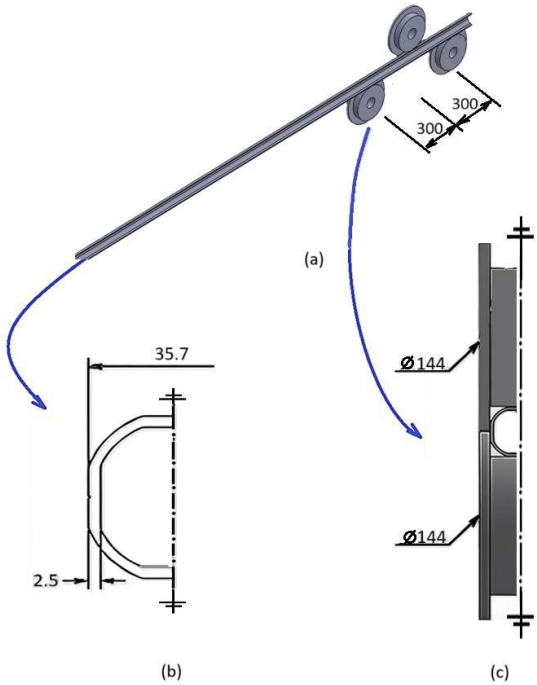

Fig. 7. Profile 3: (a) computational domain; (b) profile dimensions considering symmetry; and (c) rolling mill dimensions (in mm).

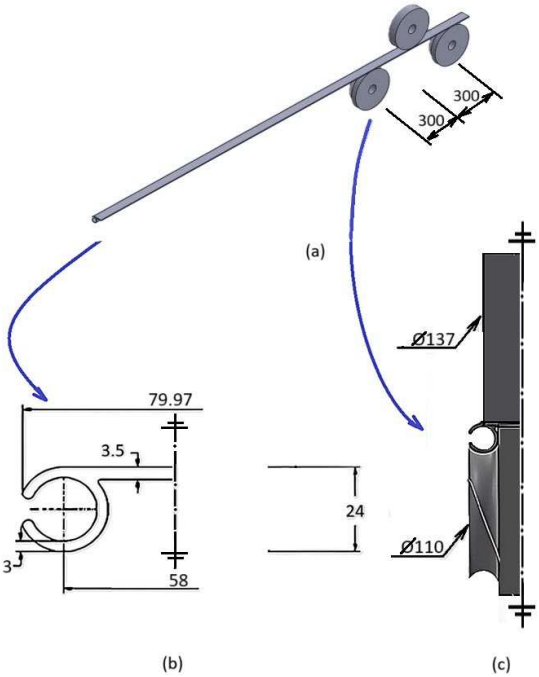

Fig. 8. Profile 4: (a) computational domain; (b) profile dimensions considering symmetry; and (c) rolling mill dimensions (in mm).

In addition, the developed computational model considers geometric and material nonlinearities, as well as surface-to-surface contact effects; these considerations are necessary due to the large deformations imposed by the roll bending process. The mechanical behavior of the extruded 6061-T6 aluminum was defined in the numerical model by a multilinear relationship, i.e., by the real stress-strain curve provided by Souza [37], as plotted in Fig. 9. It was also taken into account the contact nonlinearities (frictional contact) since the horizontal displacement of the profile occurs through the friction existing on the contact surfaces, along with the rotation of the rollers. Regarding the material behavior, the rollers were assumed rigid, while the aluminum profile was considered flexible, since the material of the rollers of the roll bending machine have a much higher stiffness than the material of the rolled profile. It is important to note that in all simulated profiles, the horizontal distances between the rollers are the same and equal to 300 mm.

Furthermore, the researchers opted for the augmented Lagrangian algorithm. This method ensures that the constraint is satisfied by employing Lagrange multipliers instead of relying on excessively high penalty stiffness, which can lead to issues with convergence and the conditioning of the global stiffness matrix. However, using this approach results in more equilibrium iterations compared to alternative algorithms [36].

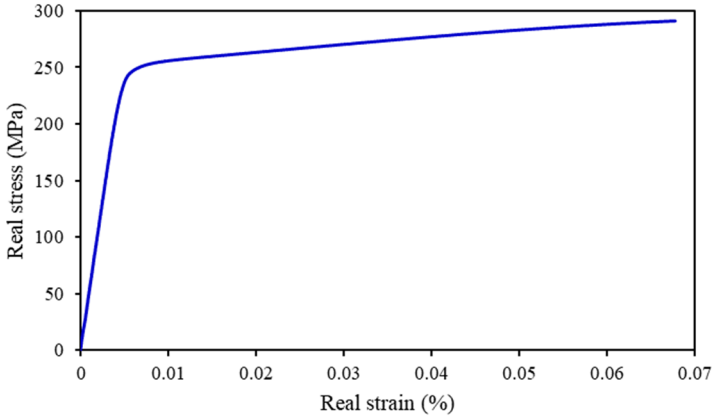

Fig. 9. Real stress-strain curve for extruded 6061-T6 aluminum [37].

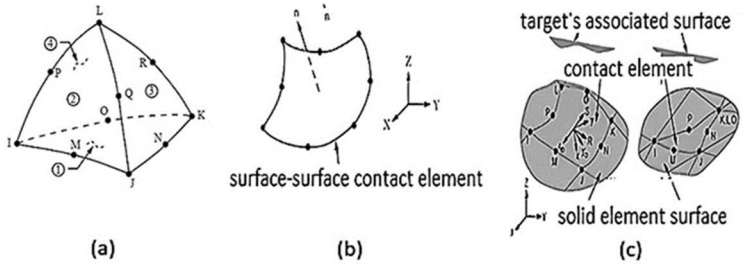

Fig. 10. Finite elements adopted in the computational modeling: (a) SOLID187; (b) CONTA174; and (c) TARGE170 [36].

Additionally, the SOLID187 finite element was used to model the aluminum profiles, based on the mesh convergence study performed by Moreira et al. [1]. The CONTA174 finite element was employed to model the contact surfaces on the aluminum profile, promoting the contact between the profile and the machine's rollers (the contact element is located on the surfaces of the SOLID187 element, and the nodes are arranged accordingly). The TARGE170 element was adopted for the rollers, with the contact stablished when the CONTA174 elements of the contact surface of the aluminum profile penetrate the TARGE170 element. Figure 10 schematically represents these finite elements used in the computational modeling of the roll bending process applied to aluminum profiles.

The SOLID187 (see Fig. 10(a)) is a three-dimensional (3D) high-order solid finite element that supports quadratic displacement behavior. The element consists of 10 nodes, each with 3 degrees of freedom, i.e., translations in the nodal x, y, and z directions. This element supports various important features such as plasticity, hyperelasticity, creep, stress stiffening, large deflections, and high deformation capacity. Due to its mixed formulation, SOLID187 allows simulating the deformation of nearly incompressible elastoplastic materials and fully incompressible hyperelastic materials. In its turn, the CONTA174 is a finite element used to represent contact and sliding between 3D target surfaces and a deformable surface defined by this element. It is suitable for 3D structural contact and coupled field analyses and can be applied for both pair-based contact and general contact. When used for pair-based contact, the target surface is defined by the type of 3D target element, known as TARGE170. In the case of general contact, the target surface can be defined by CONTA174 elements (for deformable surfaces) or TARGE170 elements (for rigid bodies only) [36].

More comprehensive details regarding the computational model used in the present study, as well as its validation based on the experimental results of Spoorenberg et al. [22], can be found in the work of Moreira et al. [1].

3. Results and Discussion

Initially, a mesh convergence test (Tables 1, 3, 5, and 7) was conducted to assess whether the results are sufficiently independent of the spatial discretization used. Therefore, the ideal mesh size is sought to find the best balance between accuracy and computational cost. The ideal mesh size is when the obtained results vary minimally with respect to mesh refinement.

For a comprehensive understanding of the results, it is necessary to clarify some essential aspects. In the Tables 2, 4, 6, and 8, the column referring to displacement is linked both to the graph and to the equation for approximate displacement prediction, both displayed in the second figure of each profile. The displacements values (D1, D2, D3, and D4) highlighted in the representation of each profile is associated with a specific equation, describing the approximate evolution of displacement in a specific region as the radius of curvature decreases. The variable *r* in the equations in the second image of each profile represents the desired radius of curvature in the roll bending process. By inputting the value of *r*, it is possible to obtain the corresponding value of the displacement, indicating the approximate resulting displacement at that radius of curvature. It is relevant to emphasize that the term "approximate displacement" is used due to performing a curve fit based on the results of numerical simulations, using predefined values of radii and displacements. Besides that, the first value in the curvature radius column of each profile corresponds to the maximum achievable radius during the roll bending process.

Another significant point in the Tables 2, 4, 6, and 8 is the relationship between the material's ultimate tensile strength (UTS) and the maximum von Mises stress ($\sigma_{\max}^{vM}$) developed during the roll bending process for each radius of curvature, resulting in a safety factor, reported in these tables. The UTS used for aluminum 6061-T6 material was 290.66 MPa [38]. In addition, as explained by Hibbeler [38], the UTS represents the maximum stress a material can withstand before structural failure occurs. In turn, the von Mises stress is a parameter used to evaluate the stress state in a material subjected to external loads. Therefore, when the ($\sigma_{\max}^{vM}$) reaches the UTS, it indicates that the material is operating at its maximum strength limit (i.e., with no safety factor), signaling a high level of stress and proximity or attainment of the structural failure point.

Table 1. Mesh convergence test for profile 1.

Mesh Size (mm)	Number of Finite Elements	Maximum Tensile Stress (MPa)	Relative Difference (%)	Processing Time
12	31491	160.42	-32.90	11 h 02 min
10	44270	213.20	-10.76	17 h 34 min
8	67085	236.13	2.40	23 h 11 min
7	84215	230.46	-2.74	33 h 57 min
6	122845	236.77	-	47 h 42 min

Table 2. Profile 1 results.

r (mm)	σ_{max}^{vM} (MPa)	Safety factor	Displacement (mm)	
			D1	D2
38588.85	248.33	1.17	2.60	1.58
14275.17	271.14	1.07	6.71	8.14
10971.68	282.00	1.03	12.98	11.39

3.1. Analysis of Profile 1

Table 1 displays the mesh convergence test results for profile 1 using the SOLID187 finite element. From the results presented in Table 1, the mesh with 67,085 finite elements was selected for the computational modeling of profile 1.

It is interesting to explain that the relative difference (*RD*) is defined between the maximum tensile stress of two successive meshes, and given by:

$$RD = \frac{100\left(M_j - M_{j+1}\right)}{M_j} \tag{1}$$

where M_j is the coarser mesh and M_{j+1} is the finer mesh. Equation (1) was used to define the converged mesh for the four studied profiles, since it is widely used in engineering problems solved with computational approaches (such as in [39-41]).

Figure 11 along with Table 2 show the obtained results of stresses and displacements for the different simulated radii of curvature in the roll bending process of profile 1, while Fig. 12 depicts the curve fitting generated for displacements D1 and D2.

Based on the results obtained for the profile 1 – a square tubular profile manufactured with aluminum 6061-T6 – presented in Figs. 11 and 12 and Table 2, several pertinent observations stand out:

i) Inverse trend between von Mises stress and radius of curvature: upon examining the data of radius of curvature and maximum von Mises stress in Table 2, there is an evident inversely proportional relationship between these two variables. As the radius of curvature decreases, the von Mises stress tends to increase gradually. Such correlation is expected, as profiles with smaller radius of curvature experience more significant displacements during the roll bending process, resulting in higher stress concentration;

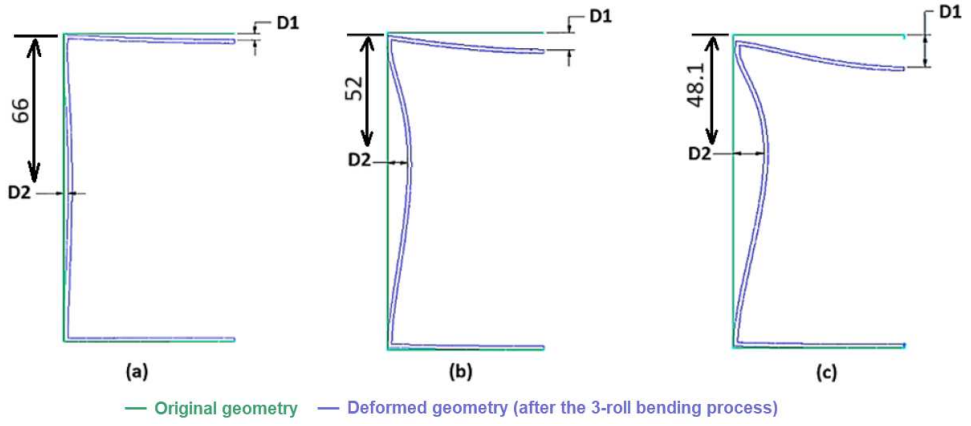

Fig. 11. Displacements for the profile 1 (in mm) when: (a) r = 38588.85 mm; (b) r = 14275.17 mm; and (c) r = 10971.68 mm.

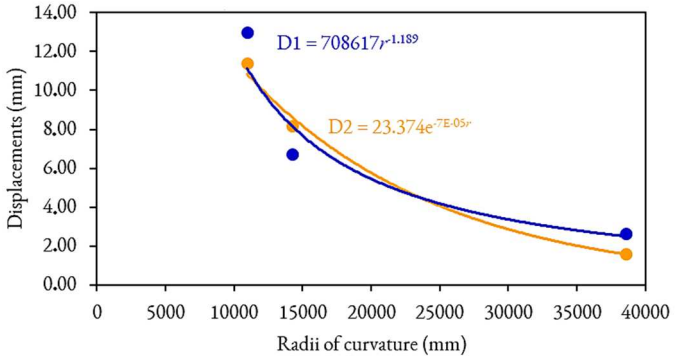

Fig. 12. Curve fitting for displacements of profile 1.

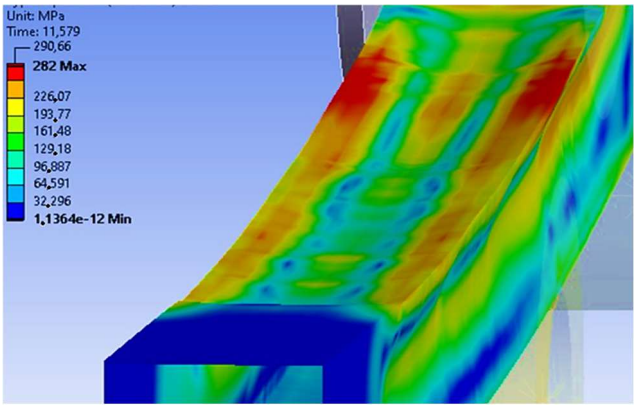

Fig. 13. The von Mises stresses distribution in the upper region of profile 1 with a radius of curvature of 10971.68 mm.

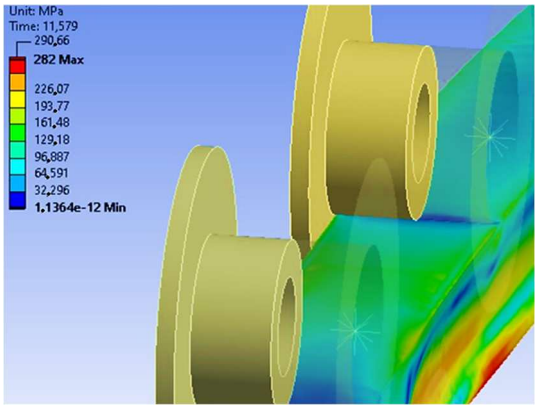

Fig. 14. The von Mises stresses distribution in the lower region of profile 1 with a radius of curvature of 10971.68 mm.

ii) Proximity to the ultimate tensile strength limit: it was noted that as the radius of curvature decreases, the von Mises stress progressively approaches the material's ultimate tensile strength limit. This indicates that the profile is approaching the structural failure point, emphasizing the importance of considering adequate safety margins when designing or using profiles with smaller radius of curvature;

iii) Practical limits of applicability: the results indicated that the profile with the largest radius of curvature exhibited a maximum von Mises stress of 248.33 MPa, representing about 85% of the material's ultimate tensile strength limit. Conversely, as the radius of curvature decreases, the von Mises stress progressively approaches the ultimate tensile strength limit, reaching its maximum value of 282.00 MPa, corresponding to approximately 97% of the material's ultimate tensile strength limit. This information is crucial for establishing practical limits of applicability of the profile, ensuring its use within safe ranges of stress and strength; and

iv) Analysis of displacements at distinct locations (D1 and D2): by inspecting the displacements generated by the roll bending process on profile 1, it is possible to establish a correspondence between these changes and the mechanical defect previously evidenced in Fig. 3. More specifically the corresponding defect is characterized as deformation in the cross-section. This suggests a direct connection between the displacements induced by the roll bending process and the manifestation of the mechanical defects identified in the profile. The analysis of displacements D1 and D2 of profile 1 provides valuable insight into the material's behavior during the roll bending process. The simulation results indicate that at larger radii of curvature, both displacements tend to be insignificant, resulting in values close to zero. This suggests lower stress concentrations and displacements in these areas, indicating that the profile is less prone to significant distortions. Conversely, at smaller radii of curvature, displacements D1 and D2 become more significant. It is important to note that the relationship between D1 and D2 does not follow a pattern; in some cases, D1 is larger, while in others, D2 exhibits higher values. However, upon analyzing the distribution of von Mises stresses, it can be observed that the regions where D1 and D2 are located coincide with the areas of highest stresses in the profile, along with the region near the highest inertia (lateral base of the profile). This phenomenon can be observed in Figs. 13 and 14. This variability between D1 and D2 highlights the complex nature of the roll bending process and its influences on stress and displacement distribution.

It is important to highlight that the items i) and ii) discussed above are also observed in the same way for the other three profiles evaluated in this work. From this reason, these specific discussions will not be reiterated in the analysis of the remaining profiles.

3.2. Analysis of Profile 2

The results obtained for the mesh convergence test performed for the profile 2, using the SOLID187 finite element, are presented in Table 3. From these results, the mesh with 16,271 elements was selected for the computational modeling of profile 2.

In Fig. 15 and Table 4 the results generated from the analysis of stresses and displacements for each radius of curvature employed during the roll bending process applied to profile 2 are presented. These results highlight the impact of curvature on the mechanical behavior of the profile, providing a detailed view of stress distributions and displacements along its structure.

Table 3. Mesh convergence test for profile 2.

Mesh Size (mm)	Number of Finite Elements	Maximum Tensile Stress (MPa)	Relative Difference (%)	Processing Time
16	3684	29.34	-9.26	00 h 21 min
12	5303	32.06	-10.98	00 h 40 min
10	7288	35.58	-4.35	00 h 56 min
8	12745	37.13	-2.65	01 h 20 min
7	16271	38.11	1.75	02 h 49 min
6	20585	37.44	-	03 h 58 min

Table 4. Profile 2 results.

r (mm)	σ_{max}^{vM} (MPa)	Safety factor	Displacement (mm)		
			D1	D2	D3
3873.56	256.02	1.14	0.62	-	-
1193.10	281.21	1.03	1.04	-	0.73
447.89	290.51	1.00	1.22	0.30	0.83
330.69	290.65	1.00	1.23	0.55	0.88

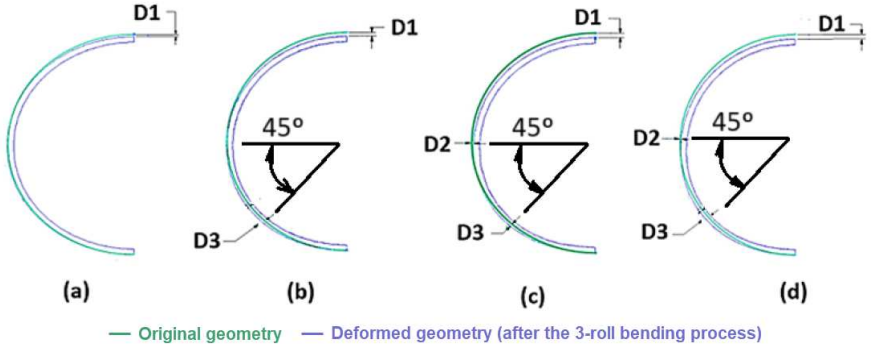

Fig. 15. Displacements for the profile 2 when: (a) r = 3873.56 mm; (b) r = 1193.10 mm; (c) r = 447.89 mm; and (d) r = 330.69 mm.

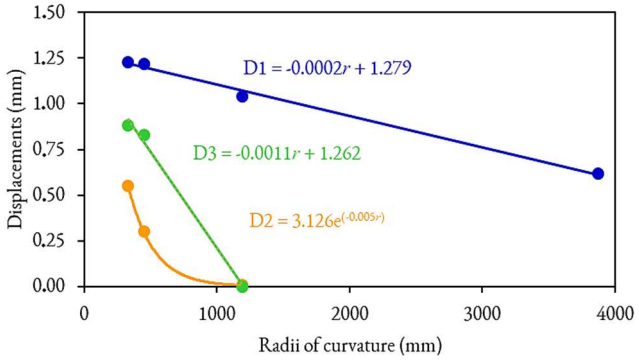

Fig. 16. Curve fitting for displacements of profile 2.

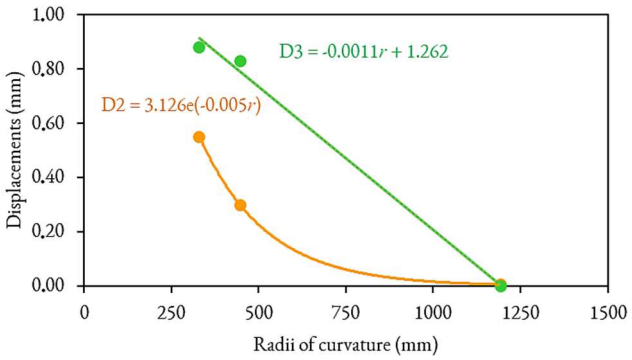

Fig. 17. Detail of curve fitting for displacements D2 and D3 of profile 2.

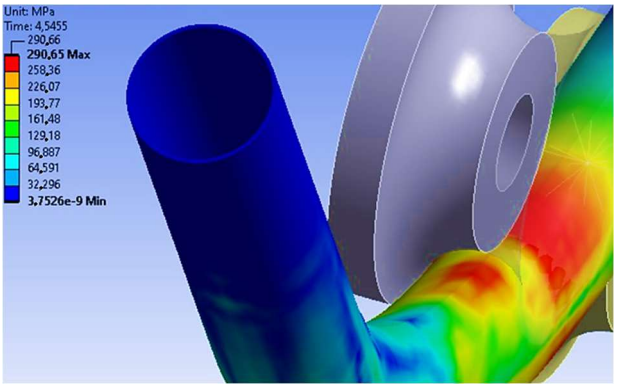

Fig. 18. The von Mises stresses distribution in the upper region of profile 2 with a radius of curvature of 330.69 mm.

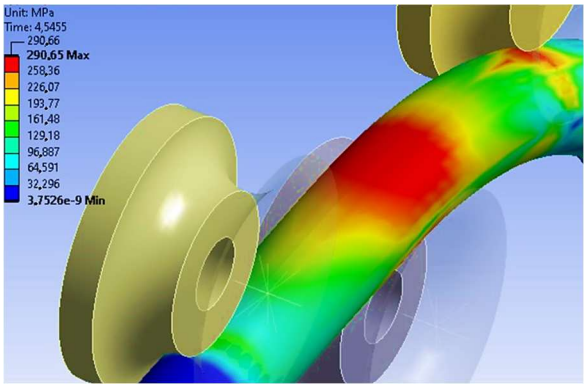

Fig. 19. The von Mises stresses distribution in the lower region of profile 2 with a radius of curvature of 330.69 mm.

Subsequently, Figs. 16 and 17 graphically illustrate the displacements obtained during the numerical simulations of profile 2. By focusing specifically on displacements, this visual representation offers a clear perspective of the displacements resulting from the application of curvature. This analysis is essential for understanding the profile's response to the forces involved in the roll bending process, highlighting areas with higher and lower magnitudes of displacement.

The analysis of the results (see Figs. 15 to 17 and Table 4) revealed essential information about the mechanical behavior of the profile 2 when subjected to the roll bending process, including:

i) Applicability limit: the results indicated that profiles with smaller radii of curvature can reach von Mises stresses that approach significantly the material's ultimate tensile strength limit. Therefore, profile 2 range between approximately 88% and 100% of the material's ultimate tensile strength limit. This aspect highlights the importance of defining practical applicability limits to ensure that profiles are used within safe ranges of stress and strength. This information is crucial for guiding the choice of curvature radii in projects requiring high strength and structural integrity; and

ii) Analysis of displacements at distinct locations (D1, D2, and D3): by examining the displacements generated by the roll bending process in profile 2, a correspondence can be established among these displacements and the mechanical defect previously evidenced in Fig. 3, known as deformation in the cross-section. A particularly intriguing discovery was the variation in displacements at different observation points (D1, D2, and D3), indicating significant differentiation in the stresses generated in distinct regions of the profile, even under the same radius of curvature. Upon analyzing the displacements at D1, D2, and D3, it is noticeable that the values of D1 are larger if compared to D2 and D3. However, when analyzing the distribution of von Mises stresses in Figs. 18 and 19, it is noticeable that the regions where D1, D2, and D3 are located do not follow this same relation; the stresses are distributed similarly in the upper and lower parts of the profile. This disparity in displacements and stresses highlights the intrinsic complexity of the material behavior during roll bending process, emphasizing the need for more detailed analyses.

Table 5. Mesh convergence test for profile 3.

Mesh Size (mm)	Number of Finite Elements	Maximum Tensile Stress (MPa)	Relative Difference (%)	Processing Time
11	6395	69.55	-37.32	00 h 31 min
10	6945	95.52	-20.53	00 h 42 min
9	7660	115.12	-4.71	01 h 21 min
8	11787	120.54	-2.33	02 h 13 min
6	17223	123.35	1.49	03 h 09 min
5	22492	121.51	-	04 h 33 min

Table 6. Profile 3 results.

r (mm)	σ_{max}^{vM} (MPa)	Safety factor	Displacement (mm)			
			D1	D2	D3	D4
3476.70	260.40	1.12	0.17	-	-	-
1026.20	273.49	1.06	0.80	0.28	0.31	-
553.80	286.64	1.01	1.28	0.42	0.40	0.32
381.90	290.65	1.00	2.59	0.73	0.40	0.51

3.3. Analysis of Profile 3

From the mesh convergence test carried out for the profile 3, one can observe that is indicated a mesh with 17223 finite elements of type SOLID187, as reported in Table 5.

After that, Fig. 20 together with Table 6 presented the results for stresses and displacements associated with different radii of curvature adopted during the numerical simulation of the roll process applied to the profile 3. Moreover, Figs. 21 and 22 depict the curve fitting for the displacements D1, D2, D3, and D4 illustrated in Fig. 20 and occurred throughout the simulated roll bending process for profile 3.

From the results obtained for profile 3 (see Figs. 20 to 22 and Table 6), some important aspects regarding the stress and displacement behaviors due to the different radii of curvature in roll bending process can be highlighted:

i) Applicability limit: the results indicate that the profile with the largest radius of curvature exhibited a maximum von Mises stress of 260.40 MPa, representing 89.59% of the material's ultimate tensile strength. As the radius of curvature decreases, the von Mises stress progressively approaches the ultimate tensile strength, reaching its maximum value of 290.65 MPa, practically coinciding with the material's ultimate tensile strength. These values are crucial for establishing the profile's applicability limits, ensuring its use within safe stress ranges; and

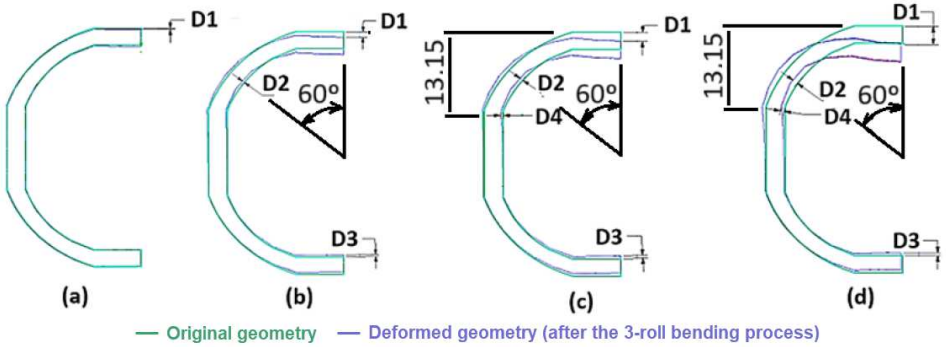

Fig. 20. Displacements for the profile 3 (in mm) when: (a) r = 3476.70 mm; (b) r = 1026.20 mm; (c) r = 553.80 mm; and (d) r = 381.90 mm.

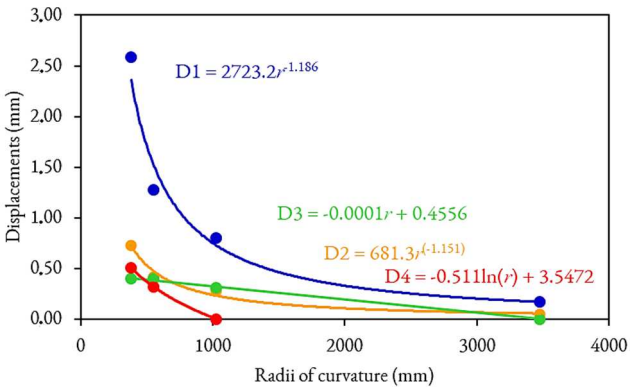

Fig. 21. Curve fitting for displacements of profile 3.

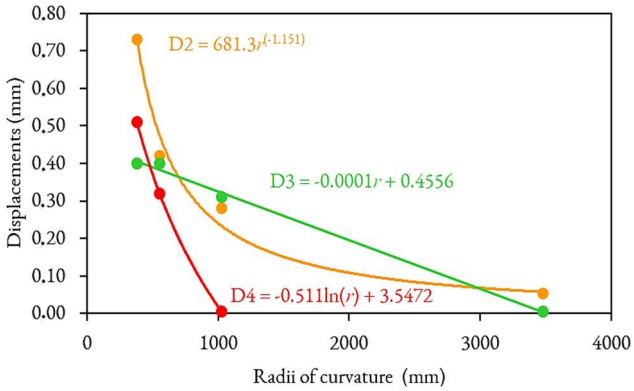

Fig. 22. Detail of curve fitting for displacements D2, D3, and D4 of profile 3.

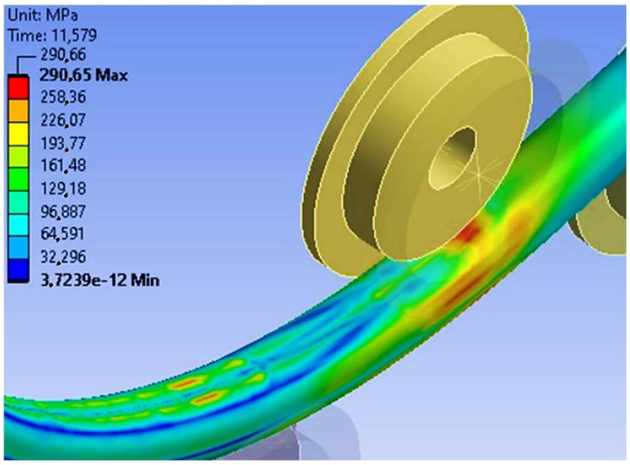

Fig. 23. The von Mises stresses distribution in the upper region of profile 3 with a radius of curvature of 381.90 mm.

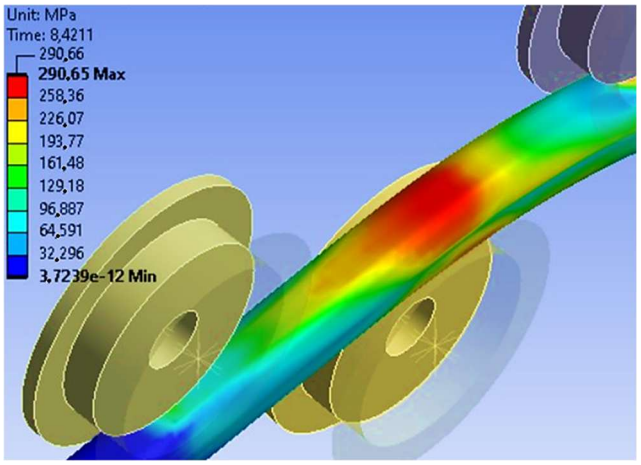

Fig. 24. The von Mises stresses distribution in the lower region of profile 3 with a radius of curvature of 381.90 mm.

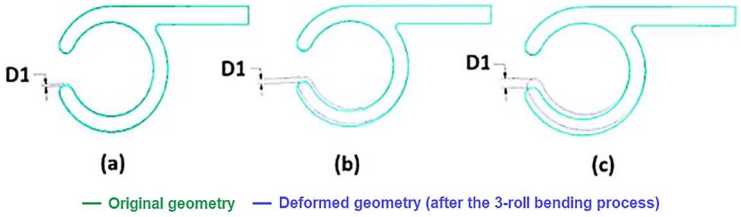

Fig. 25. Displacements for the profile 4 when: (a) r = 1301.19 mm; (b) r = 659.58 mm; and (c) r = 413.95 mm.

ii) Analysis of displacements at distinct locations (D1, D2, D3, and D4): similar to profiles 1 and 2, the corresponding defect in this case is designated as deformation in the cross-section. When examining the displacements at different points on the profile 3, an interesting pattern emerges. At D1, D2, D3, and D4, different levels of displacement are observed, especially as the radius of curvature decreases. This suggests that displacements are more pronounced in regions near the sharper curvatures of the profile. Besides, it is possible to note that displacements are more prominent in the region of D1 (the upper part of the profile) compared to D2, D3, and D4. However, when analyzing the distribution of von Mises stresses in Figs. 23 and 24, it is noticeable that the regions where D1, D2, D3, and D4 are located coincide with the regions of higher stresses. However, they do not follow the same proportion as the displacements, since the stresses are distributed similarly in these regions of the profile. This disparity in displacements illustrates the intrinsic complexity of the material's behavior during the roll bending process, emphasizing the importance of focused and detailed analyses.

3.4. Analysis of Profile 4

Table 7 shows the mesh convergence test results for profile 4 using the SOLID187 finite element.

From Table 7, it is possible to infer that the mesh with 74177 finite elements is adequate to perform the numerical simulations of the roll bending process of the profile 4.

Figure 25 and Table 8 report the results of the analyses conducted regarding the stresses and displacements for three different radii of curvature considered for the roll bending process of profile 4. In addition, Fig. 26 presents the curve fitting to the displacements suffered by profile, due to these different radii of curvature.

Table 7. Mesh convergence test for profile 4.

Mesh Size (mm)	Number of Finite Elements	Maximum Tensile Stress (MPa)	Relative Difference (%)	Processing Time
18	5218	9.80	-92.97	03 h 07 min
13	7023	18.91	-12.44	04 h 33 min
10	10020	21.27	-13.72	05 h 04 min
8	15981	24.18	-7.253	06 h 17 min
7	19202	25.94	2.49	09 h 29 min
6	24657	25.29	-5.99	12 h 01 min
4	74177	26.81	-2.37	16 h 15 min
3	177277	27.44	-	25 h 55 min

Table 8. Profile 4 results.

r (mm)	σ_{max}^{vM} (MPa)	Safety factor	Displacement (mm)
			D1
1301.19	264.82	1.10	0.40
659.58	283.54	1.03	0.95
413.95	290.63	1.00	1.72

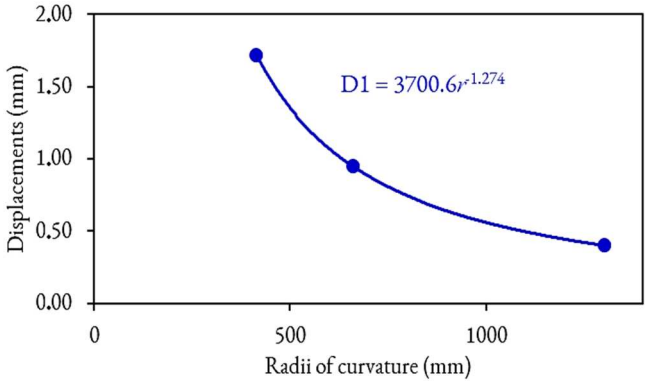

Fig. 26. Curve fitting for displacements of profile 4.

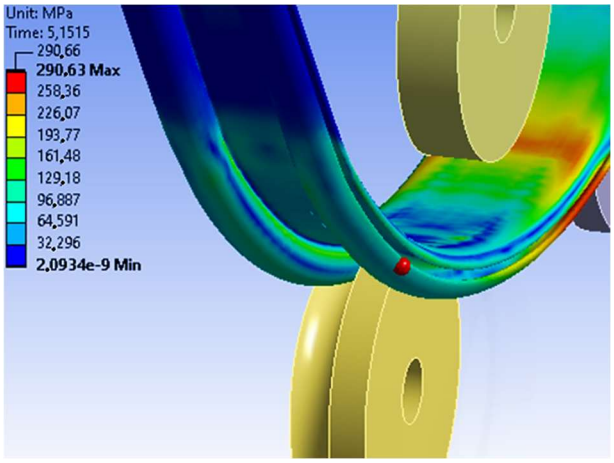

Fig. 27. The von Mises stresses distribution in the upper region of profile 4 with a radius of curvature of 413.95 mm.

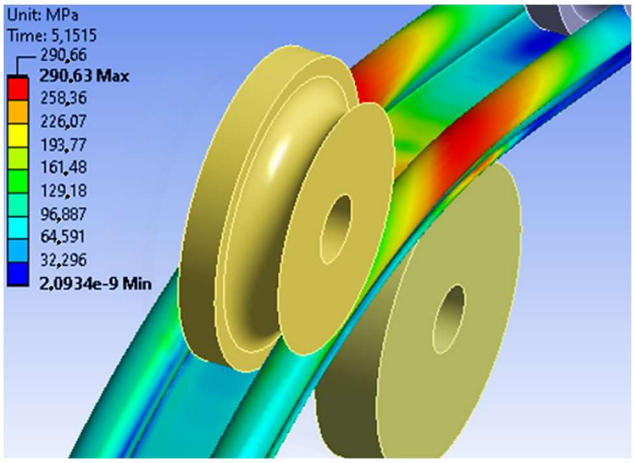

Fig. 28. The von Mises stresses distribution in the lower region of profile 4 with a radius of curvature of 413.95 mm.

When exploring the results related to profile 4 (see Figs. 25 and 26 and Table 8), relevant aspects emerge concerning the intensity of stresses and displacements, considering the variation in the radius of curvature. These results provide a detailed analysis of the structural responses of this profile under different forming conditions, as follows:

i) Applicability limit: the results indicates that a wider radius of curvature results in a maximum von Mises stress of 264.82 MPa, representing approximately 91% of the material's strength limit. On the other hand, when the radius of curvature is significantly smaller, the von Mises stress reaches 290.63 MPa, practically reaching the material's strength limit. These results define the safe range of applicability of the profile 4 under specific loading conditions originated in the roll bending process; and

ii) Analysis of displacements at a specific location (D1): unlike the other profiles studied, only one region of profile 4 suffered displacement (see Fig. 25) caused by the roll bending process. As identified in the other profiles, this mechanical defect is characterized by a deformation in its cross-section (see Fig. 3).

These observations suggest a peculiar distribution of stresses and displacements in region D1. Analyzing Figs. 27 and 28, it is possible to observe that there are two regions subjected to high stresses, the upper region of the profile and the region at D1. However, it is noted that the area subjected to high stresses at D1 is considerably larger than the upper area subjected to the same stresses, which explains the disparity in displacement results. In contrast, other regions in the profile manifested considerably lower stresses and displacements compared to D1. This dissimilarity in displacements reiterates the intrinsic complexity of the material's behavior when subjected to the roll bending process.

The notable singularity of displacement at D1 in profile 4 emphasizes the importance of localized and meticulous analyses for each profile configuration. This result highlights that different profile geometries can result in distinct displacement patterns, which have important implications for design optimization and selection of roll bending parameters.

4. Conclusions

Based on the numerical study carried out, one can conclude that the comparative investigation of the effects of different radii of curvature on extruded 6061-T6 aluminum profiles during the bending process is of paramount importance for understanding their mechanical behaviors. The obtained results demonstrate significant variations in stress and displacement distributions, directly influencing the safety and structural integrity of the profiles. Therefore, the relevance of computational models based on the finite element method to accurately predict such distributions is emphasized.

It was observed that all analyzed profiles exhibited the same relationship between radius of curvature and von Mises stress: as the radius of curvature decreases, the von Mises stress tends to increase gradually, reaching values practically equal to the material's ultimate tensile strength. This indicates that the profiles are approaching the point of structural failure, underscoring the importance of considering adequate safety margins when designing or using profiles with smaller radii of curvature.

The research not only highlights the importance of stress distribution but also of the displacements generated during the roll bending process. The variation in displacements at different observation points reveals significant differences in the stresses generated in different regions of the profiles, even under the same radius of curvature. By analyzing each profile individually, it is possible to identify that the quantity and region of displacements are distinct factors for each profile. For instance, profiles 3 and 4

presented a considerable discrepancy in these factors: while the profile 3 presents four distinct displacement regions (D1, D2, D3, and D4 – see Fig. 20), the profile 4 presents only one displacement (D1 – see Fig. 25), suggesting greater dimensional stability for profile 4. This displacements analysis provides important information about the material's behavior during forming, highlighting the intrinsic complexity of the roll bending process. In addition, this analysis forms the basis for structural design improvements, enabling a more accurate consideration of the regions most vulnerable to stress concentrations and displacements. A more focused approach to analysis and optimization can be adopted, ensuring that the most critical areas of the profiles are strengthened and dimensioned properly.

It is also important to highlight that the variation in displacements is attributed to the interaction among the profile geometry, the radius of curvature, and other mechanical factors. This observation underscores the importance of analyzing each profile specifically, considering the peculiarities of its cross-sectional shapes and loading conditions. Furthermore, a broad understanding about the variations in displacements in different regions of the profile is crucial for project optimization and to prevent excessive displacements that may compromise structural integrity.

In this sense, the numerical analysis conducted in this study provides a basis for enhancing the roll bending process, allowing the identification of critical stress and displacement regions and ensuring adequate safety margins to prevent structural failures in extruded 6061-T6 aluminum profiles.

In future works, other complex profiles manufactured with different materials will be investigated by means the numerical approach employed in the present work, as well as to perform studies addressed to the geometrical optimization of these profiles. Besides that, opportunities emerge for future research in the field of aluminum profile rolling, such as exploring the influence of different aluminum alloy compositions on the rolling process, which can provide insights for selecting more suitable materials in challenging marine environments. Additionally, extending the research to evaluate the corrosion resistance of these alloys after the rolling process may be highly relevant to ensure the durability of the structures. It is also suggested to expand the scope of the investigation to examine the effects of varying operational parameters, such as rolling speed and temperature, on the mechanical behavior of aluminum profiles. A more thorough analysis of these aspects can provide a comprehensive understanding of the optimal conditions for the rolling process, contributing to the optimization of method performance and efficiency.

Author Contributions

All authors equally contributed to the research. The manuscript was written through the contribution of all authors. All authors discussed the results, reviewed, and approved the final version of the manuscript.

Acknowledgments

The authors thank TechnNOVA and Gustavo Henrique O. Silva for providing the necessary technical information and support.

Conflict of Interest

The authors declared no potential conflicts of interest concerning the research, authorship, and publication of this article.

Funding

The authors thank the National Council for Scientific and Technological Development (CNPq) for the financial support to the action (Processes: 308396/2021-9 and 309648/2021-1).

Data Availability Statements

The datasets generated and/or analyzed during the current study are available from the corresponding author on reasonable request.

References

[1] Moreira, M.S., Souza, J.H.C., Guilherme, C.E.M., Isoldi, L.A., Computational model validation of the rolled shapes calendaring process, *Ciência e Natura*, 45, 2023, e74455.
[2] Kissell, J.T., Ferry, R.J., *Aluminum Structures: A Guide to Their Specifications and Design 2ª ed.*, John Wiley Sons, 2010.
[3] Sun, X., Han. X., Dong, C., Li, X., *Applications of Aluminum Alloys in Rail Transportation*, IntechOpen, 2021. http://dx.doi.org/10.5772/intechopen.96442.
[4] Nguyen, D.T., Kim, Y.S., Jung, D.W., Finite element method study to predict spring-back in roll-bending of pre-coated material and select bending parameters, *International Journal of Precision Engineering and Manufacturing*, 13, 2012, 1425–1432.
[5] Fragassa, C., Modelling the Viscoelastic Response of Ceramic Materials by Commercial Finite Elements Codes, *FME Transactions*, 44, 2016, 58-64.
[6] Seo, J.H., Tyne, C.J.V., Moon, Y.H., Effect of Roll Configuration on the Leveling Effectiveness of Tail-Up Bent Plate Using Finite-Element Analysis, *Journal of Manufacturing Science and Engineering*, 138(7), 2016, 071004.
[7] Pavlovic, A., Fragassa, C., Modelling the viscoelasticity of ceramic tiles by finite element, *AIP Conference Proceedings*, 1736, 2016, 020174.
[8] Ghiabakloo, H., Kim, J., Kang, B.S., An efficient finite element approach for shape prediction in flexibly-reconfigurable roll forming process, *International Journal of Mechanical Sciences*, 142–143, 2018, 339–58.
[9] Graça, A., Vincze, G., A Short Review on the Finite Element Method for Asymmetric Rolling Processes, *Metals*, 11(5), 2021, 762.
[10] Yousefi, M., Rahnama, S., Nia, M.F., Theoretical and Experimental Investigation on Mechanical Behavior of Aluminum to Aluminum Tubular Bonded Lap Joint under Pure Torsion and a Finite Element Comparison with Hybrid Rivet/Bonded Joint, *Journal of Applied and Computational Mechanics*, 8(2), 2022, 485-492.
[11] Pater, Z., The Application of Finite Element Method for Analysis of Cross-Wedge Rolling Processes—A Review, *Materials*, 16(13), 2023, 4518.
[12] Elmoghazy, Y.H., Safaei, B., Sahmani, S., Finite Element Analysis for Dynamic Response of Viscoelastic Sandwiched Structures Integrated with Aluminum Sheets, *Facta Universitatis, Series: Mechanical Engineering*, 21(4), 2023, 591-614.
[13] Zhu, X., Wang, X., Wu, H., Calculation method and analysis of residual stress in the strip bending roller straightening process, *Scientific Reports*, 14, 2024, 9149.
[14] Liang, J., Han, C., Li, Y., Yu, K., Liang, C., Study on deformation difference between the contact zone and the non-contact zone of the flexible 3D stretch bending profile and roller dies based on pre-stretching amount, *The International Journal of Advanced Manufacturing Technology*, 108, 2020, 3579–3589.
[15] Payrebrune, K.M., Relation of kinematics and contact forces in three-body systems with a limited number of particles, *Mechanical Engineering*, 20, 2022, 95–108.
[16] Zhao, X., Huang, S., Yin, S., Yang, J., Yang, Z., Tao, G., Wen, Z., Influence of unilateral low adhesion on transient wheel-rail rolling contact and wheel

damages, *International Journal on the Science and Technology of Friction, Lubrication and Wear*, 530–531, 2023, 205053.
[17] Hao, C., Wang, P., Xu, J., Liu, Y., Chen, J., An, B., Yi, Q., Wang, S., Investigation of transient wheel-rail interaction and interface contact behaviour in movable-point crossing panel, *Vehicle System Dynamics*, 62(5), 2024, 1103–1121.
[18] Hansen, N.E., Jannerup, O., Modelling of Elastic-Plastic Bending of Beams Using a Roller Bending Machine, Journal of Engineering for Industry, *Transactions of the ASME*, 101, 1979, 304-310.
[19] Gandhi, A.H., Raval, H.K., Mathematical Modelling and Finite Element Simulation of Pre-Bending Stage of Three-Roller Plate Bending Process, *International Manufacturing Science and Engineering Conference, MSEC*, Evanston, IIIinois, USA, 2008.
[20] Tailor, V.K., Gandhi, A.H., Finite Element Analysis of Deformed Geometry in Three-Roller Plate Bending Process, *In Proceedings of the 2008 International Manufacturing Science and Engineering Conference (MSEC2008)*, October 7-10, Evanston, Illinois, USA, 2008.
[21] Merklein, M., Hagenah, H., Cojutti, M., Investigations on Three-Roll Bending of Plain Tubular Components, *Key Engineering Materials*, 410-411, 2019, 325-334. Trans Tech Publications.
[22] Spoorenberg, R.C., Snijder, H.H., Hoenderkamp, J.C.D., Finite element simulations of residual stresses in roller bent wide flange sections, *Journal of Constructional Steel Research*, 67, 2010, 737-747.
[23] Zhao, W., Liao, T.W., Kompotiatis, L., Stress and Springback Analyses of API X70 Pipeline Steel Under 3-Roller Bending via Finite Element Method, *Acta Metallurgica Sinica (English Letters)*, 30, 2017, 470-482.
[24] Feng, Z., Champliaud, H., Modeling and Simulation of Asymmetrical Three-Roll Bending Process, *Simulation Modelling Practice and Theory*, 19, 2011, 1913-1917.
[25] Thakare, Prafull, S., Sandip, M., Salodkar, Handa, C.C., Desenvolvimento de um modelo matemático para o deslocamento do rolo superior de uma dobradeira de três rolos usando análise dimensional, *Anais da Conferência Internacional sobre Manufatura Inteligente e Automação*, Springer, Cingapura, 2019.
[26] Thanasoulas, I.D., Gantes, C.J., Numerical investigation on the residual stresses of roller-bent circular-hollow-sections, *Journal of Constructional Steel Research*, 164, 2020, 105777.
[27] Zhigulev, G.P., Skripalenk, M.N., Fadeev, V.A., Skripalenko, M.M., Modeling of Deformation Zone During Plate Stock Molding in Three-Roll Plate Bending Machine, *Metallurgist*, 64(3-4), 2020, 349-355.
[28] Kamas, T., Sarıkaya, M., Explicit dynamics finite element analyses of asymmetrical roll bending process, *International Advanced Researches and Engineering Journal*, 5(3), 2021, 435-443.
[29] Mazur, T., Rucki, M., Gutsalenko, Y., Accuracy Analysis of the Curved Profile Measurement with CMM: a Case Study, *Facta Universitatis, Series: Mechanical Engineering*, 21(1), 2023, 121-135.
[30] Chapra, S.C., Canale, R.P., *Numerical Methods for Engineers (Métodos numéricos para engenheiros) (7ª ed.)*, McGraw Hill, 2014.
[31] Mercury A., Fanelli, P., Giorgetti, F., Rubino, G., Stefanini, C., Experimental and numerical analysis of roll bending process of thick metal sheets, *IOP Conference Series: Materials Science and Engineering*, 1038, 2021, 012067.
[32] Zhou, W., Zhou, H., Zhang, R., Pei, Y., Fang, D., Measuring residual stress and its influence on the properties of porous ZrO2ZrO2+Ni ceramic, *Material Science and Engineering: A*, 622, 2015, 82-90.
[33] Tekkaya, A.E., Chatti, S., Dobra Tubes, Profiles. *CIRP Encyclopedia of Production Engineering*, Springer, Berlin, Germany, 2014.
[34] Selvaggio, A., Dirksen, U., Tekkaya, A.E., Schikorra, M., Kleiner, M., Increasing profile bending production accuracy with computational intelligence, *Evolve Computar*, 17, 2009, 561-576.
[35] Eurocode 9 - Design of Aluminium Structures, European Committee for Standardization, 2020.
[36] Ansys Inc., *ANSYS User's Manual: Analysis of Systems*, 2022.
[37] Souza, J.H.C., *Stamping fundamentals course*, TechnNOVA, 2022.
[38] Hibbeler, R.C., *Mechanics of Materials 11º ed.*, Pearson, 2022.
[39] Pinto, V.T., Rocha, L.A.O., Fragassa, C., dos Santos, E.D., Isoldi, L.A., Multiobjective Geometric Analysis of Stiffened Plates under Bending through Constructal Design Method, *Journal of Applied and Computational Mechanics*, 6, 2020, 1438-1449.
[40] Moreira, R., de Escobar, C.C., Isoldi, L.A., Davesac, R., Rocha, L.A.O., dos Santos, E.D., Numerical Study and Geometric Investigation of Corrugated Channels Subjected to Forced Convective Flows, *Journal of Applied and Computational Mechanics*, 7(2), 2021, 727-738.
[41] Del Aghenese, A.P., Naldi, C., Rocha, L.A.O., Isoldi, L.A., Prolo Filho, J.F., Biserni, C., Dos Santos, E.D., Geometrical investigation of forced convective flows over staggered arrangement of cylinders employing constructal design, *International Communications in Heat and Mass Transfer*, 155, 2024, 107553.

ORCID iD

Mauricio da Silva Moreira https://orcid.org/0000-0002-7945-048X
Carlos Eduardo Marcos Guilherme https://orcid.org/0000-0001-5356-6524
João Henrique Corrêa de Souza https://orcid.org/0000-0002-5181-0201
Elizaldo Domingues dos Santos https://orcid.org/0000-0003-4566-2350
Ana Pavlovic https://orcid.org/0000-0003-2158-1820
Liércio André Isoldi https://orcid.org/0000-0002-9337-3169

How to cite this article: da Silva Moreira M., et al., Influence of Curvature Radius on Mechanical Behavior of Extruded 6061-T6 Aluminum in Roll Bending, *J. Appl. Comput. Mech.*, xx(x), 2024, 1–14. https://doi.org/10.22055/jacm.2024.46183.4473